

Effect of interface on magnetic exchange coupling in Co/Ru/Co trilayer: from ab-initio simulations to micromagnetics

Sergiu Arapan, Jan Priessnitz, and Dominik Legut
*VSB - Technical University of Ostrava**

Alexander Kovacs, Harald Oezelt, David Böhm, Markus Gusenbauer, and Thomas Schrefl
Universität für Weiterbildung Krems

Interfaces play a substantial role for the properties function structured magnetic materials and magnetic multilayers. Modeling the functional behavior of magnetic materials requires treatment of the relevant phenomena at the device level. Properties that arise from the electronic structure and spin dynamics at the atomistic level have to be properly transferred into a continuum level treatment. In this work we show how Co/Ru/Co three layers can be simulated with the continuum theory of micromagnetism, if interface coupling energies and bulk intrinsic properties are derived from the results of ab-initio and spin dynamics simulations at different temperatures.

I. INTRODUCTION

In ferromagnetic materials spins or magnetic moments are coupled. This coupling is described by a quantum mechanical effect called exchange. It is the main physical effect/reason for ferromagnetism. The exchange energy is the energy that misaligned spins/magnetic moments/electrons have to pay and reason that in equilibrium more aligned ones are energetically favored. How strong spins/magnetic moments are coupled is determined by either the exchange integral J_{ij} , depending on the overlap of wave-functions of two unpaired electrons or the more classical exchange constant A which is the pre-factor for the following exchange energy density $e_{\text{ex}} = A|\nabla\mathbf{m}|^2$, where \mathbf{m} denotes the magnetization direction. Magnetic phenomena are studied through their dynamic behavior, and the systems are, usually, too large to be investigated at the atomistic level. Thus, the magnetic properties are predicted within the micromagnetic description. In the framework of micromagnetism, all relevant energies are expressed in terms of the unit magnetization vector which is a continuous function of space $\mathbf{m}(\mathbf{x})$. The micromagnetic approach is based on the Landau-Lifshitz-Gilbert (LLG) equation for $\mathbf{m}(\mathbf{x})$, and its solutions require the knowledge of appropriate structural and micromagnetic properties. One approach is to determine these parameters from the intrinsic magnetic properties at the atomic level, by mapping the results of the electronic structure calculations to a Heisenberg model. A shortcoming of this method is that the intrinsic magnetic properties are derived for ideal bulk systems, while the real materials are never perfect. Another aspect is that classical micromagnetism does not treat thermal fluctuations explicitly. The intrinsic magnetic properties are assumed to depend on temperature. The magnetic moment per unit volume is replaced by its average temperature dependent value which results in the tempera-

ture dependent spontaneous magnetization $M_s(T)$. Similarly, the magnetocrystalline anisotropy constant $K(T)$ and the exchange constant $A(T)$ are temperature dependent. They are normally measured at temperature T , at which the specimen is observed.

In this work, we show how these temperature dependent parameters can be derived for a system with "imperfections" from ab-initio simulations and atomistic spin dynamics. As an example, we study the coupling of the two Co layers in a Co/Ru/Co trilayer. Depending on the Ru layer thickness this coupling is either ferromagnetic or antiferromagnetic [1, 2]. For the micromagnetic simulations of the trilayer, we assume an interlayer exchange constant between the two Co layers $J_{\text{Co,Co}}(T)$, which is temperature dependent. Its value is derived by matching the interface spin configuration obtained from spin dynamic simulations and micromagnetic theory.

In our simulations, we want to compute the spin configuration of a domain wall at the Co|Ru interface. We will compute the domain wall structure as a function of temperature using both spin dynamics simulations and micromagnetic simulations. FIG. 1 shows the expected magnetization distribution across the Ru layer in hexagonal close packed (hcp) Co.

Ab-initio computations are capable of providing insights to the zero Kelvin properties such as the total magnetic moment of a super-cell, the exchange between atomic sites, and the magneto-crystalline anisotropy energy. The latter is derived by comparing energies between states in which the magnetization/spins/moments are aligned with an underlying crystalline easy-axis direction and orthogonal to that axis. The zero-temperature intrinsic properties derived from ab-initio simulations serve as input for atomistic spin dynamic simulations. These simulations solve the Landau-Lifshitz-Gilbert equation for classical spins at the fixed atom sites. Temperature is included through a thermal fluctuation field whose strength is derived from the fluctuation-dissipation theorem. Large-scale systems are typically simulated by micromagnetic simulations. Classical micromagnetism is a continuum theory. Instead of discrete spins, the func-

* sergiu.arapan@gmail.com

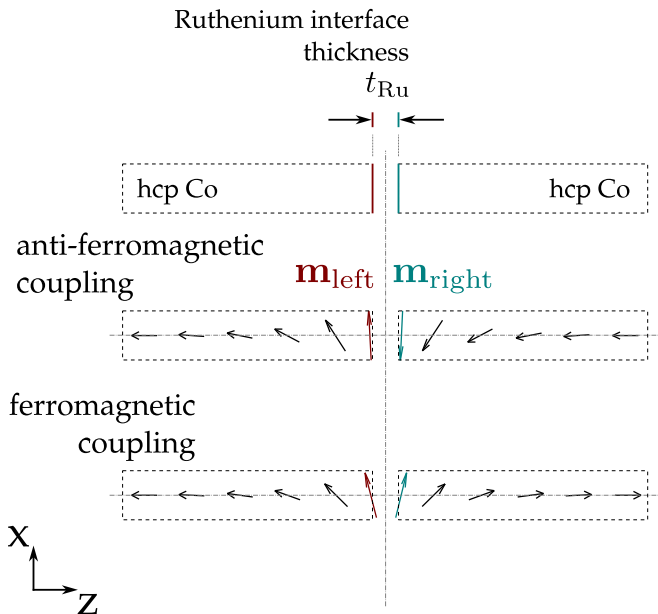


FIG. 1. Simulation of magnetic moment configurations for domain walls across a Ru layer in hcp Co. Top: Schematics of the Co/Ru/Co trilayer. Center: Expected magnetization profile of a domain wall for anti-ferromagnetic coupling across the Ru layer. Bottom: Expected magnetization profile for ferromagnetic coupling across the Ru layer.

tion $\mathbf{m}(\mathbf{x})$ describes the magnetic state. However, in this work we treat the exchange interactions of ferromagnets across interfaces. The vector field $\mathbf{m}(\mathbf{x})$ is not continuous but may show a jump across the interface [3].

We aim to match those at the length scales of atomistic simulations and that of continuum theory quantitatively and try to offer a guideline on how to calibrate your micromagnetic simulations with your gained knowledge from ab-initio and spin dynamics for magnetic systems including interfaces.

This paper is structured as follows:

First we present the overall methodology (II). We summarize the procedure (IIA) applied to obtain the intrinsic material properties for micromagnetic simulations of Co/Ru/Co trilayers. We show how we derived the exchange interaction energy per atom J_{int} across the Ru layer (IIB) using ab-initio simulations. This is an input parameter for spin dynamics simulations (IIC) in detail. From the results of spin dynamics simulations, we derived the input parameters of micromagnetic simulations (IID).

Then we present the results (III). We show the temperature-dependent domain wall profiles in Co/Ru/Co trilayers computed with spin dynamics simulations for varying Ru thickness (IIIA). We derive the temperature dependent intrinsic magnetic properties for micromagnetic simulations from the spin dynamics results (IIIB). We use the temperature dependent intrinsic magnetic properties in micromagnetic simulations of the domain wall profiles for different Ru thickness (IIIC).

In addition, we should mention that, in this work, we mainly focus on the exchange between ferromagnetic layers and how it is affected by the Ru spacer. At this stage we do not take into account the changes in the spin magnetic moment of Co atoms at the Co|Ru interface, as well as the variation of the magneto-crystalline anisotropy of the Co/Ru/Co systems with the width of the Ru spacer. We also do not consider the change of the magneto-crystalline anisotropy due to structural phase transition at elevated temperatures.

Finally we draw conclusions (IV).

II. METHODOLOGY

A. Overview

For the micromagnetic simulations of domain wall profiles of Co/Ru/Co trilayers as a function of temperature, we need the temperature dependent exchange constant $A(T)$ of Co, the temperature dependent anisotropy constant $K(T)$ of Co, and the interlayer exchange constant $J_{\text{Co,Co}}(T)$ between the two Co layers across the Ru interface. In order to derive these parameters we apply the following procedure.

1. Ab-initio simulations

Ab-initio simulations give the exchange interaction energy between pairs of magnetic moments J_{ij} in bulk Co and the exchange energy between atom pairs across the Ru interface J_{int} . In this work we use the J_{ij} values previously computed by Turek et al. [4] and only compute J_{int} . From the interaction energies we compute the zero temperature exchange constant $A(0)$ of bulk Co.

2. Spin dynamic simulations

Spin dynamic simulations use the exchange energies J_{ij} and J_{int} and the anisotropy energy k_{u} per atom as input. The value of k_{u} is taken from literature [5] and corresponds to the zero temperature anisotropy constant $K(0)$ of bulk hexagonal closed packed (hcp) Co. We show the temperature dependent anisotropy constant $K(T)/K_0$ scales like $(M_{\text{s}}(T)/M_{\text{s}}(0))^3$. Using computed domain wall profiles for bulk Co, we obtain $A(T)$ and show that $A(T)/A(0)$ scales like $(M_{\text{s}}(T)/M_{\text{s}}(0))^2$. Spin dynamic simulations of magnetization profiles of Co/Ru/Co trilayers show a jump in the average magnetic moment across the Ru layer. We define the angle φ_{int} between the average of magnetic moments of Co touching the left side of the Ru layer and the average of the magnetic moments of the Co atoms touching the right side of the Ru layer.

3. Micromagnetism

We use micromagnetic theory to derive the temperature dependent exchange coupling $J_{\text{Co,Co}}(T)$

across the Ru layer from $K(T)$, $A(T)$, and φ_{int} . Temperature dependent magnetization profiles in Co/Ru/Co layers can now be calculated using micromagnetic theory and the temperature dependent bulk properties $K(T)$, $A(T)$, and the temperature dependent coupling constant $J_{\text{Co,Co}}(T)$.

4. Validation

We compare the temperature dependent magnetization profiles in Co/Ru/Co layers computed with spin dynamics simulations and micromagnetic simulations.

The above scheme for parameter passing from the ab-initio calculations, spin dynamics simulations to micromagnetic simulations is schematically shown in FIG. 2.

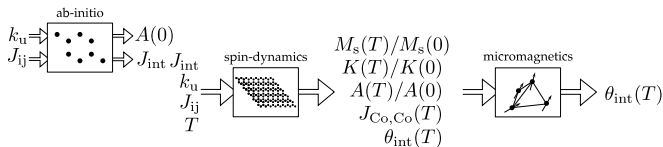


FIG. 2. Parameter passing between ab-initio calculations, spin dynamics simulations and micromagnetic calculations, see (II A) for more details.

B. Ab-initio calculations

Electronic structure calculations of $\text{Co}(d_{\text{Co}})|\text{Ru}(d_{\text{Ru}})$ systems were done with the Vienna Ab initio Simulation Package (VASP) software (version 6.2.1). VASP is a plane-wave basis set implementation [6, 7] of the Density Functional Theory within the Projector Augmented Wave (PAW) approximation. [8] Calculations were performed using the generalized gradient approximation of Perdew, Burke, and Ernzerhof (PBE) [9] to the exchange-correlation part of the energy functional. We used PAW PBE potentials version 5.4 with 15 and 14 valence electrons for Co and Ru, respectively. The size of the plane-wave basis set was determined by an energy cut-off $\text{ENCUT} = 439.857 \text{ eV}$, which is 50 % larger than the default one. The reciprocal space was sampled with a uniform mesh of k points [10] with a separation between the k points $\text{KSPACING} = 0.1 \text{ \AA}^{-1}$. For total energy summation, we used the Methfessel-Paxton method [11], with $\text{ISMEAR} = 1$ and the width of smearing $\text{SIGMA} = 0.025 \text{ eV}$. Electronic convergence was set to $\text{EDIFF} = 10^{-7} \text{ eV}$, and geometry optimization was carried out until the norms of all Hellman-Feynman forces [12] were less than 10^{-3} eV/\AA . Equilibrium structure parameters were obtained by performing a set of geometric optimizations (ion positions and cell shape) at volumes within a 5 % range about equilibrium and fitting the energy vs volume data, $E = E(V)$, to the Rose-Vinet equation of state. [13] $\text{Co}(d_{\text{Co}})|\text{Ru}(d_{\text{Ru}})$ multilayers were modeled as periodic supercells of the hcp unit cell, with the c -axis

oriented along the x -direction. A supercell comprises of two Co layers, with layer width $0.8 \text{ nm} \leq d_{\text{Co}} \leq 2.6 \text{ nm}$ (from 4 to 13 Co atomic layers) each, separated by a few Ru atomic layers (1, 2, and 3) as shown in FIG. 3.

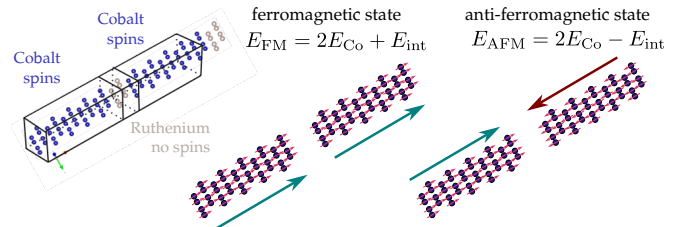


FIG. 3. Sketch of a Co/Ru/Co slab. Both Co bulk parts are configured in two different states i) into a ferromagnetic (FM) state and ii) into an anti-ferromagnetic (AFM) state. The calculated total energies $E_{\text{AFM/FM}}$ of the AFM/FM configurations can be factorized in the contributions from the two bulk-like Co slabs E_{Co} , and exchange interaction energy at the interface E_{int} .

From the calculated total energies, we can now calculate an effective exchange interaction energy per atom following

$$E_{\text{int}} = (E_{\text{FM}} - E_{\text{AFM}})/2 \quad (1)$$

$$E_{\text{int}} := 2 \cdot N_x \cdot N_y \cdot J_{\text{int}} \quad (2)$$

where $E_{\text{AFM/FM}}$ are the total energies of the AFM/FM configurations. E_{int} represents the exchange interaction of the left bulk with the right bulk across the Ru interface.

According to the Heisenberg model, we will add E_{int} to the total energy when the spins across interface are oriented in parallel, and subtract E_{int} if the spins are oriented anti-parallel. Thus, E_{int} can be calculated by subtracting the total energies E_{FM} and E_{AFM} .

With the number of spins in x - and y -direction at the interface, N_x and N_y respectively, we can calculate the interface energy contribution per atom by dividing E_{int} by the number of atom pairs forming the interfacial exchange interactions. This is the dimension of the supercell in the x - and y -direction times 2, because there are actually 2 Co|Ru interfaces in our arrangement. The resulting coupling energies for 1, 2 and 3 monolayers of Ru as a function of the width of Co layers are shown in Fig.4. For the ASD calculations we have chosen the following values for the effective coupling between Co pairs separated by a Ru spacer: $J_{\text{int},1} = -1.376 \text{ mRy}$ ($-3 \times 10^{-21} \text{ J}$), $J_{\text{int},2} = -0.7301 \text{ mRy}$ ($-1.59 \times 10^{-21} \text{ J}$), and $J_{\text{int},3} = 0.3011 \text{ mRy}$ ($0.656 \times 10^{-21} \text{ J}$) for a Ru spacer of 1, 2, and 3 atomic layers, respectively.

Following Moreno et al. [5], we compute the zero temperature exchange constant of bulk hcp Co parallel to the c -axis using

$$A(0) = \frac{1}{4V_{\text{at}}} \sum_i J_{0i} \cdot (r_i - r_0)^2 \quad (3)$$

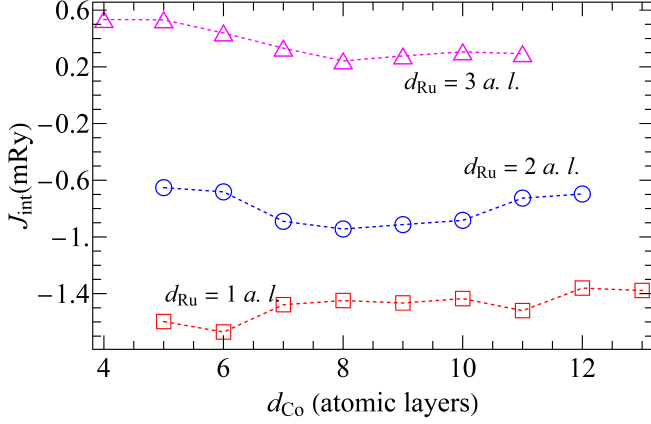


FIG. 4. Effective Heisenberg interactions J_{int} between Co atoms separated by a Ru spacer as a function of the width of Co layers d_{Co} and Ru spacer d_{Ru} .

where i iterates over all neighboring atoms of 0-th atom, J_{0i} is the exchange interaction energy, r_i is the atom positions along the c -axis, and $V_{at} = 1.1 \times 10^{-29} \text{ m}^3$ is the volume per atom. This gives $A(0) = 52.78 \text{ pJ/m}$.

C. Spin dynamic simulations

We use the classical spin dynamics method to bridge the gap between density functional theory, which calculates supercells of up to hundreds of atoms, and micromagnetics, which simulates systems on the micrometer scale containing billions of atoms, albeit on the continuum level. Our spin dynamics usage lies somewhere in the middle, simulating around 1 million atoms. This is necessary to capture the collective phenomena which arise due to finite temperature and determine the temperature dependence of the magnetic properties of the material, such as the saturation magnetization $M_s(T)$, magnetocrystalline anisotropy $K(T)$, exchange stiffness $A(T)$ and, in turn, the domain wall width $\delta_{DW}(T)$.

The simulated system is described by the following Hamiltonian:

$$\mathcal{H} = - \sum_{i,j} J_{ij} \vec{S}_i \cdot \vec{S}_j - \sum_i k_u (\vec{S}_i \cdot \vec{e}_k)^2$$

where J_{ij} is the exchange interaction energy between pairs of magnetic moments i and j , k_u is the magnetocrystalline anisotropy energy, \vec{e}_k is the easy-axis direction $-\vec{e}_k = (0, 0, 1)$ throughout this work $-\vec{e}_k$ and \vec{B}_{ext} is the external magnetic field vector. \vec{S}_i is the normalized moment vector at i -th site ($|\vec{S}_i| = 1$). Note that each pair is counted twice $-J_{ij}$ is halved to account for double counting.

Exchange interaction energies J_{ij} are taken from ab initio calculations by Turek et al. [4]. 38 nearest unique

exchange interaction pairs were taken into account, corresponding to a distance cutoff of about 1 nm.

The anisotropy energy per atom is taken from Moreno et al. [5] $k_u = 5.83 \cdot 10^{-24} \text{ J/atom}$, corresponding to a macroscopic magnetocrystalline anisotropy constant of $K(0) = 0.547 \text{ MJ/m}^3$.

In the bulk hexagonal-closely-packed Co system, the exchange interaction between i -th and j -th spin is defined as $J(\vec{r}_{ij}) - J$ only depends on the relative position of spin pairs, thanks to translational symmetry of the system.

In this work we simplify the actual Co/Ru/Co interface by replacing the influence of the Ru atoms with an effective exchange interaction J_{int} $-$ from section II B. Apart from this effective exchange interaction, there are no other interactions between atoms of the two bulks. Thus we write for the Hamiltonian for the Co/Ru/Co trilayer:

$$\begin{aligned} \sum_{i,j} J_{ij} \vec{S}_i \cdot \vec{S}_j = & \sum_{i,j \in C_{BL}} J(\vec{r}_{ij}) \vec{S}_i \cdot \vec{S}_j + \\ & \sum_{i,j \in C_{BR}} J(\vec{r}_{ij}) \vec{S}_i \cdot \vec{S}_j + \\ & \sum_{i \in C_{IL}, j \in C_{IR}} J_{int} \vec{S}_i \cdot \vec{S}_j \delta(\vec{r}_i - \vec{r}_j - \vec{r}_{int}) + \\ & \sum_{i \in C_{BL}, j \in C_{BR}} (-1) \cdot J(\vec{r}_{ij} - \vec{l}_z) \vec{S}_i \cdot \vec{S}_j \end{aligned}$$

where C_{BL} , C_{BR} are sets containing spins in the left and right bulk, respectively, C_{IL} and C_{IR} are sets of spins on the left and right side of the interface and J_{int} is the specific energy of exchange interaction across the interface calculated from bilinear coupling in section II B. \vec{r}_{int} is the relative position of the nearest neighbors across the interface and \vec{l}_z is the size of the simulation domain in the z -direction. Note that $C_{IL} \subset C_{BL}$, $C_{IR} \subset C_{BR}$ and $C_{BL} \cup C_{BR}$ contains all spins.

The first two terms describe the exchange interactions inside the left and right Co bulk. The third term stands for the interaction across the Ru interface. The fourth term stands for the antiperiodic boundary condition in the z -direction, which helps to pin the domain wall in the middle of the simulation domain. Periodic boundary conditions in the (x,y) -direction are also employed in this model, but not explicitly mentioned in the Hamiltonian above.

The atomistic spin dynamics approach is based on the Landau-Lifschitz-Gilbert (LLG) equation for individual spins:

$$\frac{d\vec{S}_i}{dt} = - \frac{\gamma}{1 + \alpha^2} \vec{S}_i \times \vec{H}_i^{\text{eff}} - \frac{\gamma\alpha}{1 + \alpha^2} \vec{S}_i \times (\vec{S}_i \times \vec{H}_i^{\text{eff}})$$

where γ is the gyromagnetic ratio, α is the Gilbert damping parameter and \vec{H}_i^{eff} is the effective field experienced by i -th spin. To introduce temperature T , a

stochastic Gaussian field $\vec{b}_i(t)$ with variance of $\sqrt{\frac{2\alpha k_B T}{\Delta t \gamma \mu_B}}$ is added to the effective field:

$$\vec{H}_i^{\text{eff}} = -\frac{d\mathcal{H}}{d\vec{S}_i} + \vec{b}_i(t)$$

where Δt is the simulation timestep. A spin dynamics simulation is then formally just an integration of the LLG equation. In this work, Heun's method is used for numerical integration with a timestep Δt small enough to keep the integration error negligible. The damping rate was chosen as $\alpha = 0.05$ based on the speed of convergence. The choice of damping parameter does not influence the domain wall width, since it is measured in the equilibrated state.

The cross section of the simulation domain is chosen to be large enough such that the thermal noise does not destroy the domain wall. The length is chosen such that the entire domain wall profile is simulated. In this work, the simulation domain consists of $50 \times 50 \times 240$ unit cells for hcp Co. Each unit cell contains 2 Co atoms at fractional coordinates $(0, 0, 0)$ and $(1/3, 1/3, 1/2)$. The simulation domain for the CoRuCo system is constructed by altering the original hcp Co simulation domain: first, a simulation domain of $60 \times 60 \times 240$ hcp Co unit cells is created, then n central layers of atoms are removed to account for the Ru interface, and then the pairwise exchange interactions at the interface are modified.

The main result of the spin dynamics stage in this work is the magnetization profile along the z-direction $M(z) \in \mathbb{R}^3$, which is calculated as the average of all spins in the individual hcp layers.

All spin dynamics calculations were carried out by our unpublished and in-house developed software. A summary of the input parameters for the spin dynamics simulations of hcp Co is given here.

- lattice constant $a = 2.47 \text{ \AA}$ and $c/a = \sqrt{8/3}$ of a hcp system
- exchange interactions are taken from ab initio calculations by I. Turek et al. [4] – 38 unique exchange interaction pairs were taken into account, corresponding to a distance cutoff of about 10 \AA . This set of exchange interactions corresponds to an exchange constant value of about $A(0) = 5.278 \times 10^{-11} \text{ J/m}$.
- the anisotropy per atom is taken from Moreno et al. [5] $k_u = 5.83 \cdot 10^{-24} \text{ J/atom}$, corresponding to macroscopic constant of $K(0) = 0.547 \cdot 10^6 \text{ J/m}^3$
- values of exchange stiffness and anisotropy written above yield a zero-Kelvin domain wall width of $\delta_{DW} = 31.35 \text{ nm}$ when using the formula $\delta_{DW} = \pi \sqrt{A/K}$
- reduced magnetic moment for Co – no experimental magnetization units are involved

D. Micromagnetism

Micromagnetism [14] is a continuum theory. The energy functional is expressed in terms of the unit magnetization vector $\mathbf{m}(\mathbf{x})$, which is a continuous function of position \mathbf{x} . We now derive the micromagnetic energy of the domain configurations shown in FIG. 1. We assume translational symmetry in the xy plane. The magnetization vector only with the position in z direction. In our approach we neglect magnetostatic interactions. There is no energy difference between a Bloch or a Néel wall [15]. We restrict the vector \mathbf{m} to lie in the xz plane and describe its direction with the angle φ from the positive z axis. We start with the energy of the domain wall in bulk Co:

$$E(\varphi) = \int_a^b \left(A \left(\frac{d\varphi}{dz} \right)^2 + K \sin^2 \varphi \right) dz \quad (4)$$

For a simple domain wall $\varphi(a) = \pi$ and $\varphi(b) = 0$. In order to express the energy of a domain wall across a Co/Ru/Co trilayer, we split the energy (4) into two parts and add a surface energy term:

$$E_{\text{wi}}(\varphi) = \int_a^0 \left(A \left(\frac{d\varphi}{dz} \right)^2 + K \sin^2 \varphi \right) dz + \int_0^b \left(A \left(\frac{d\varphi}{dz} \right)^2 + K \sin^2 \varphi \right) dz - J_{\text{Co,Co}} (\mathbf{m}_{\text{left}} \cdot \mathbf{m}_{\text{right}}) \quad (5)$$

The last term considers the coupling across the Ru layer. It is the interface energy expressed in terms of the magnetization vectors \mathbf{m}_{left} and $\mathbf{m}_{\text{right}}$ left and right of the interface, respectively. We can write the interface energy in terms of the interface angle

$$E_{\text{int}} = -J_{\text{Co,Co}} \cos(\varphi_{\text{int}}) \quad (6)$$

with

$$\varphi_{\text{int}} = \varphi_{\text{left}} - \varphi_{\text{right}}. \quad (7)$$

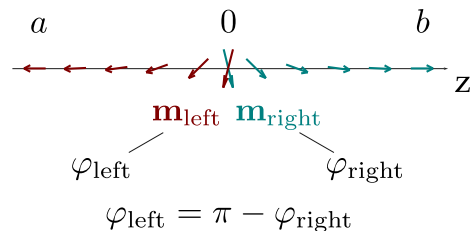


FIG. 5. Magnetization configuration at a ferromagnetic interface.

From the magnetization configuration in FIG. 5 we see that we can use symmetry to express φ_{right} in terms of φ_{left}

$$\varphi_{\text{right}} = \pi - \varphi_{\text{left}} \quad (8)$$

The interface energy is

$$E_{\text{int}} = -J_{\text{Co,Co}} \cos(2\varphi_{\text{left}} - \pi). \quad (9)$$

or

$$E_{\text{int}} = J_{\text{Co,Co}} \cos(2\varphi_{\text{left}}). \quad (10)$$

Owing to symmetry that the twist of the magnetization in the left and the right part consumes the same amount of energy. Therefore, we can write for the total energy (see also FIG. 5):

$$E_{\text{wi}}(\varphi) = 2 \int_a^0 \left(A \left(\frac{d\varphi}{dz} \right)^2 + K \sin^2 \varphi \right) dz \quad (11)$$

$$+ J_{\text{Co,Co}} \cos(2\varphi(0)) \quad (12)$$

For the functional

$$E(\varphi) = \int_a^0 \left(e \left(\varphi(z), \frac{d\varphi(z)}{dz} \right) \right) + E_{\text{int}}(\varphi(0)) \quad (13)$$

the Euler Lagrange equation is

$$\frac{\partial e}{\partial \varphi} - \frac{d}{dz} \left(\frac{\partial e}{\partial \frac{d\varphi}{dz}} \right) = 0 \quad (14)$$

The surface energy E_{int} at $z = 0$ leads the following boundary condition

$$\frac{dE_{\text{int}}}{d\varphi} + \frac{\partial e}{\partial \frac{d\varphi}{dz}} = 0. \quad (15)$$

The Euler Lagrange equations in micromagnetics and the boundary conditions arising from surface energies are discussed in [16] (see equations I.44 to I.47 in [16]). For our problem we can write the following relations.

$$e = 2A \left(\frac{d\varphi}{dz} \right)^2 + 2K \sin^2 \varphi \quad (16)$$

$$E_{\text{int}} = J_{\text{Co,Co}} \cos(2\varphi(0)) \quad (17)$$

$$\frac{\partial e}{\partial \varphi} = 4K \sin \varphi \cos \varphi \quad (18)$$

$$\frac{\partial e}{\partial \frac{d\varphi}{dz}} = 4A \frac{d\varphi}{dz} \quad (19)$$

$$\frac{dE_{\text{int}}}{d\varphi} = -2J_{\text{Co,Co}} \sin(2\varphi(0)) \quad (20)$$

With the above equations we rewrite (14)

$$4K \sin \varphi \cos \varphi = 4A \frac{d^2 \varphi}{dz^2} \quad (21)$$

$$2K \sin \varphi \cos \varphi = 2A \frac{d^2 \varphi}{dz^2} \quad (22)$$

$$\frac{d}{d\varphi} (K \sin^2 \varphi) = 2A \frac{d^2 \varphi}{dz^2} \quad (23)$$

We multiply (23) with $d\varphi/dz$ and integrate (see [16] equation I.38)

$$K \sin^2 \varphi(0) - K \sin^2 \varphi(z) = A \left(\frac{d\varphi}{dz} \Big|_0 \right)^2 - A \left(\frac{d\varphi}{dz} \Big|_z \right)^2 \quad (24)$$

At $z = -\infty$ the first term on the left hand side and the first term on the right hand side of (24) vanish as we are in the center of the magnet. Following the arguments in [16], we obtain

$$K \sin^2 \varphi(z) = A \left(\frac{d\varphi}{dz} \right)^2 \quad (25)$$

We now have a closer look at the boundary condition at $z = 0$. From (15) we obtain with (19) and (20)

$$-2J_{\text{int}} \sin(2\varphi(0)) + 4A \frac{d\varphi}{dz} \Big|_0 = 0 \quad (26)$$

From (25) we get

$$\frac{d\varphi}{dz} = \pm \sqrt{\frac{K}{A}} \sin \varphi \quad (27)$$

In our setting $\frac{d\varphi}{dz} < 0$ (see Figure 5). Therefore we take the right hand side of (27) with the minus sign and insert it into (26). At $z = 0$ we have

$$-2J_{\text{Co,Co}} \sin(2\varphi) - 4\sqrt{AK} \sin \varphi = 0 \quad (28)$$

With $\sin(2\varphi) = 2 \sin(\varphi) \cos(\varphi)$ we obtain

$$-4J_{\text{Co,Co}} \sin \varphi \cos \varphi - 4\sqrt{AK} \sin \varphi = 0. \quad (29)$$

We now evaluate equation (29) at $z = 0$. Using $\varphi_{\text{left}} = \varphi(0)$ we can write for $\varphi_{\text{left}} \neq 0$ we obtain

$$J_{\text{Co,Co}} \cos \varphi_{\text{left}} = -\sqrt{AK} \quad (30)$$

and can express the angle of the magnetization at the interface in terms of the bulk temperature dependent properties $A(T)$ and $K(T)$ and the temperature dependent interface coupling constant $J_{\text{Co,Co}}(T)$

$$\cos \varphi_{\text{left}} = -\frac{\sqrt{AK}}{J_{\text{Co,Co}}}. \quad (31)$$

The jump of the z -component of the magnetization across the interface, Δm_z was computed by averaging the spin dynamic results near the interface. Eq. 31 can be expressed with that jump as

$$J_{\text{Co,Co}} = \pm \frac{\sqrt{AK}}{\Delta m_z / 2}. \quad (32)$$

In the results section (III B), we will use equation (32) to obtain the temperature dependent coupling constant $J_{\text{Co,Co}}(T)$ from the interface angle φ_{int} , which was computed by spin dynamics simulations, and the bulk properties $A(T)$ and $K(T)$.

FIG. 6 illustrates the jump of the magnetization across the interface for ferromagnetic coupling of the two Co layers in comparison to a conventional domain wall.

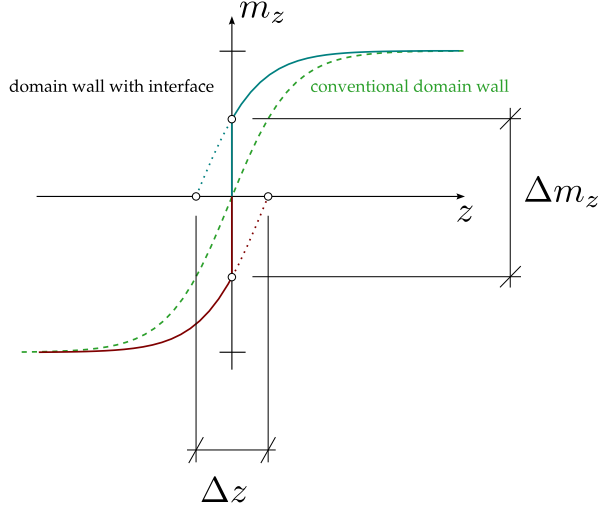


FIG. 6. Illustration of a conventional domain wall and the magnetization distribution of a Co/Ru/Co trilayer with ferromagnetic coupling. The jump in the magnetization Δm_z is used to compute the temperature dependent interface coupling constant for micromagnetics $J_{\text{Co,Co}}$.

III. RESULTS

A. Domain wall profiles from spin dynamics

In the first stage, we use spin dynamics to calculate temperature-dependent domain wall properties in bulk hcp Co and compare with previous results by [5]. The spin dynamics calculation starts with an initial configuration where the left half of the spins is $\vec{S} = (0, 0, -1)$ and the right half is $\vec{S} = (0, 0, 1)$. The simulation then runs for 2,400,000 steps and the initial configuration relaxes into equilibrated domain walls.

The magnetization profile of the averaged configuration should then follow the shape of hyperbolic tangens for the z component of the unit magnetization vector

$$m_z(z) = m_s \tanh(\pi(z - z_0)/\delta_{\text{DW}}) \quad (33)$$

where $m_s = M_s(T)/M_s(0)$ is the reduced temperature dependent magnetization, z_0 is the domain wall center, and δ_{DW} is the domain wall width. The simulated magnetization profile is then fitted into this equation in order to obtain values for the free parameters m_s , z_0 and δ_{DW} . The magnetization spin-dynamics profiles, their

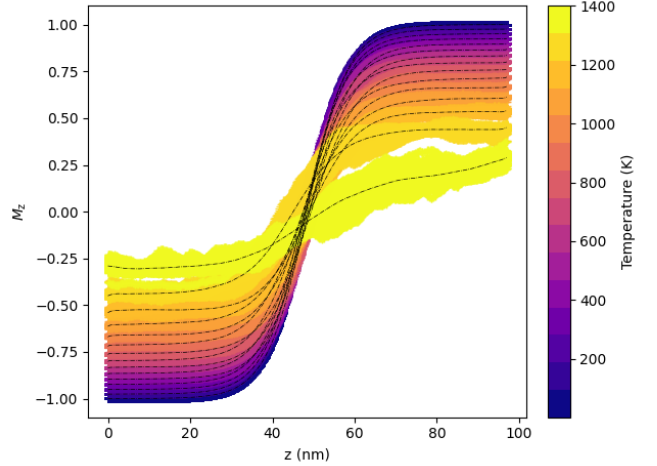


FIG. 7. Magnetization configurations after relaxation steps for different temperatures of hcp Co bulk. Colored regions show the averaged magnetization over one atomic Co layer of around 100 separate spin-dynamics simulations. The dotted lines highlight the average of those profiles for each specific temperature.

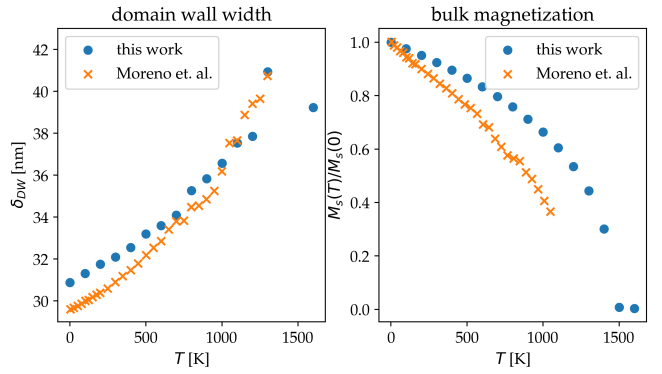


FIG. 8. Temperature dependence of domain wall width and saturation magnetization in hcp Co extracted via fit of 33. Results from Moreno et. al [5] shown for comparison.

average profiles over temperature and the results of this fitting are shown in FIG. 7 and FIG. 8. In this work, the zero-temperature domain wall width is larger than in [5], but increases more slowly with temperature. Also, the saturation magnetization decreases more slowly with temperature and indicates a Curie temperature of about $T_C \approx 1500$ K, compared to $T_C = 1300$ K in [5]. This is caused by a different input set of exchange interactions.

Calculating domain wall properties in the Co/Ru/Co trilayer with spin dynamics is performed analogically to that in bulk hcp Co. The initial configuration of the system is set according to sign of the interface exchange coupling. In case of 1 and 2 Ru layers, all spins are set to $\vec{S} = (0, 0, 1)$ and the system relaxes into an antiferromagnetic domain wall. In case of 3 Ru layers, spins in the left bulk are set to $\vec{S} = (0, 0, -1)$, spins in the right

bulk are set to $\vec{S} = (0, 0, 1)$, and the system relaxes into a conventional domain wall. The calculation is set to run for 800,000 steps. The resulting averaged magnetization profiles are shown in FIG. 9. The left most image shows the magnetization profile for one monolayer of Ru atoms separating the two Co slabs. The exchange coupling across the Ru layer is antiferromagnetic. For two monolayers Ru the antiferromagnetic coupling strength is reduced by about a factor of two. The corresponding magnetization profile is shown in the center of FIG. 9. For three monolayers of Ru atoms, the coupling is ferromagnetic. The domain wall, which shows a jump of the magnetization at the interface, is given in the right most image.

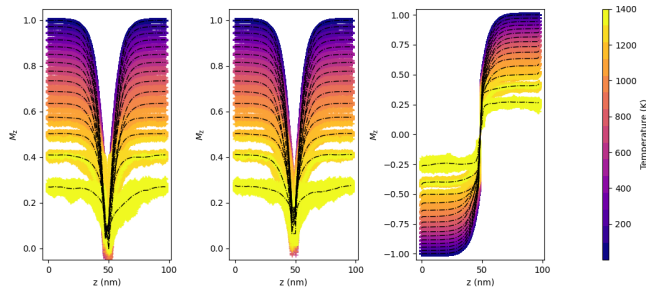


FIG. 9. Magnetization profiles across the Co/Ru/Co system for various temperatures and Ru interface thickness. Left: Ru layer thickness is 1 atomic layer, the coupling across the layer is antiferromagnetic; Center: Ru layer thickness is 2 atomic layers, the coupling across the layer is antiferromagnetic; Right: Ru layer thickness is 3 atomic layers, the coupling across the layer is ferromagnetic. The dot-dashed lines highlight the average of those profiles for each specific temperature.

B. Intrinsic properties for micromagnetics

The acquisition of all temperature dependent intrinsic material properties of hcp Co bulk follows the temperature dependence of the saturation magnetization M_s .

The spin dynamics method was used to calculate temperature dependence of magnetocrystalline anisotropy $K(T)$. We initially start with all spins pointing into the $-z$ direction. Then we apply a positive external field and integrate the stochastic LLG equation. The field is chosen such that the magnetization reverses during the simulation time. From sampling the anisotropy energy during magnetization reversal, we obtain $E_{\text{anis}}(M_z)$. For a Stoner-Wohlfarth particle this energy curve is a parabola [17], its maximum corresponds to the anisotropy constant K times the particle volume V . The Stoner-Wohlfarth switching field is $H_{\text{sw}} = 2K/(\mu_0 M_s)$.

The simulation domain consists of $10 \times 10 \times 10$ and the initial configuration is ferromagnetic (all spins $\vec{S} = (0, 0, -1)$). An external magnetic field \vec{H}_{ext} in the $+z$ direction is turned on and the ferromagnetic configura-

tion slowly goes from $M_z = -1$ to $M_z = 1$. For sampling $E_{\text{anis}}(M_z)$ during magnetization reversal we do not need to apply an external field which is sufficiently large to cause switching during the simulation time. Here we set H_{ext} a value slightly larger than an estimate of the Stoner-Wohlfarth switching field. We approximate $M_s(T)$ with the Bloch's law

$$M_s^{\text{est}}(T) = M_s(0) \left(1 - \frac{T}{T_C}\right)^{3/2}, \quad (34)$$

where T_C is the Curie temperature. For the temperature dependence of the anisotropy we assume the Callen-Callen law [18]

$$K^{\text{est}}(T) = K(0) \left(\frac{M_s(T)}{M_s(0)}\right)^3 \quad (35)$$

We use equations (34) and (35) to approximate the Stoner-Wohlfarth switching field which is used as value for the external field for simulating magnetization reversal. We validated that varying the external magnetic field up to several times H_{sw} has negligible effect on the resulting value of anisotropy $K(T)$ which supports this approach as a valid source of temperature-dependent anisotropy, instead of having to calculate the whole hysteresis curve or employing constrained Monte Carlo techniques [19]. The anisotropy energy value is extracted

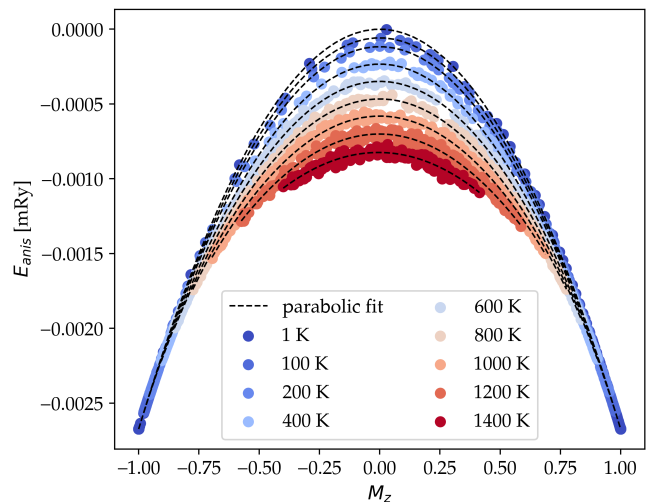


FIG. 10. Energy barrier between magnetization state $M_z = +1$ and $M_z = -1$. Achieved through sampling of anisotropy energy plotted against magnetization in the z -direction for various temperatures in bulk hcp Co. Each dot represents an average of 50,000 spin dynamics steps.

from sampling the anisotropy energy component during the spin dynamics calculation. This energy is then plotted against magnetization z -component (E_{anis} vs M_z) in FIG. 10. We can clearly see the energy barrier between $M_z = -1$ and $M_z = +1$ which corresponds to $K(T)V$. Furthermore, the data can be accurately fitted using a

parabola $E_{\text{anis}} = qM_z^2 + k$, illustrating consistency with the Stoner-Wohlfart model. The anisotropy energy was calculated as difference between highest and lowest energy in FIG. 10: $KV = \max(E_{\text{anis}}) - \min(E_{\text{anis}})$.

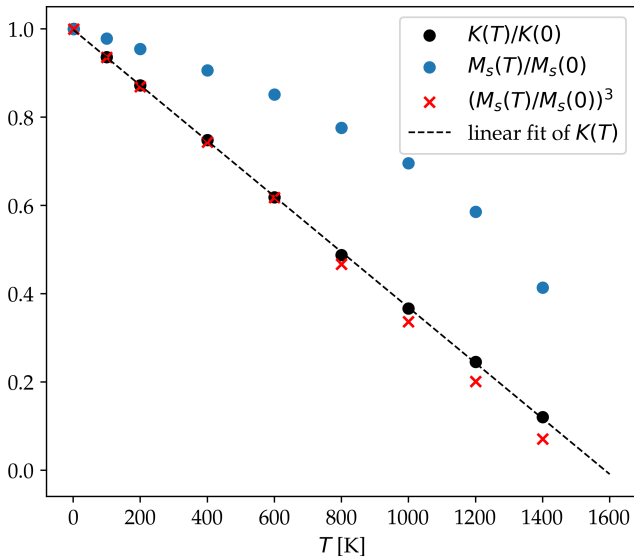


FIG. 11. Temperature dependence of calculated anisotropy, saturation magnetization, and its third power in bulk hcp Co. Saturation magnetization (blue dots), spin-dynamics estimated anisotropy constant with energy barriers (black dots), anisotropy constant following Callen-Callens law (red crosses) and a linear fit (dashed line).

FIG. 11 shows the calculated temperature dependence of $K(T)$. The anisotropy constant decreases linearly with temperature up to about 1600 K where it goes to zero. At low temperatures, it agrees exceptionally well with the Callen-Callen law. Therefore, we use equation (35) for $K(T)$ in the micromagnetic simulations.

In order to obtain the exchange constant $A(T)$, we assume a general power law

$$A_\beta(T) = A(0) \left(\frac{M_s(T)}{M_s(0)} \right)^\beta \quad (36)$$

and minimize the squared error in the domain wall width

$$F(\beta) = \sum_i \left(\delta_{\text{DW}}(T_i) - \pi \sqrt{\frac{A_\beta(T_i)}{K(T_i)}} \right)^2. \quad (37)$$

In (37) the sum is over all temperature T_i used in the spin dynamics simulations of the domain wall width shown (see FIG. 8). For minimizing (37), we used the adaptive nonlinear least-squares algorithm method (NL2SOL) by Dennis et al. [20] as implemented in the Dakota suite [21]. From nonlinear least-square fit we obtained $\beta = 2$.

FIG. 12 shows the temperature dependent intrinsic material properties for hcp Co.

In addition to the bulk properties of hcp Co, we need the coupling constant $J_{\text{Co,Co}}(T)$ across the Ru layer.

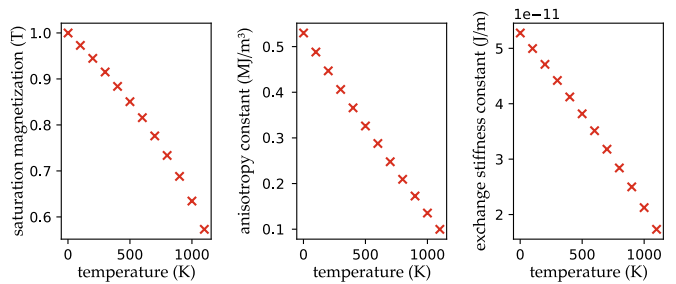


FIG. 12. Intrinsic material properties derived from spin dynamics simulations. Left: Reduced temperature dependent magnetization $M_s(T)/M_s(0)$. Center: Anisotropy constant $K(T)$. Right: Exchange constant $A(T)$.

Given the angle of the magnetic moments between the interfaces φ_{int} and with the knowledge about bulk exchange constant $A(T)$ and magnetocrystalline anisotropy $K(T)$ at specific temperature T we can use equation (32) to obtain the temperature coupling constant from the spin dynamics simulations.

Start from the spin dynamics simulation of the magnetization profiles across the Co/Ru/Co trilayer presented in section III A and compute the average magnetic moments of the Co atoms left and right of the interface. Using the notation of section II C, the average magnetic moments are

$$\mathbf{m}_{\text{left}}^{\text{spindyn}} = \frac{1}{|C_{IL}|} \sum_{i \in C_{IL}} \vec{S}_i \quad (38)$$

$$\mathbf{m}_{\text{right}}^{\text{spindyn}} = \frac{1}{|C_{IR}|} \sum_{i \in C_{IR}} \vec{S}_i \quad (39)$$

where $|C_{IL}|$ and $|C_{IR}|$ are the number of Co atoms in the sets of atoms to the left and to the right of the interface, respectively. We now compute the angle φ_{int} between the two unit vectors $\mathbf{m}_{\text{left}}^{\text{spindyn}}$ and $\mathbf{m}_{\text{right}}^{\text{spindyn}}$.

FIG. 13 shows the resulting coupling constant $J_{\text{Co,Co}}(T)$ for one, two, and three monolayers of Ru atoms between the Co layers as a function of temperature T .

In table I we show selected values for the micromagnetic input parameters.

C. Domain wall profiles from micromagnetics

We now compute magnetization profiles across Co/Ru/Co layers using micromagnetic simulations. For the simulations we use the temperature dependent properties listed in table I as input. The wall profiles are obtained by minimizing the micromagnetic energy (11) numerically.

IV. CONCLUSION

In lowest order, temperature is included in micromagnetism through temperature-dependent material param-

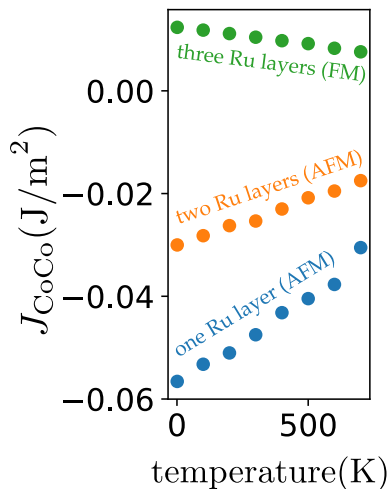


FIG. 13. The interface exchange coupling extracted from the Δm_z relation from equation (32) in units of J/m^2 .

TABLE I. Input parameters for micromagnetic simulations of Co/Ru/Co trilayers. The columns give the number Ru monolayers n , the temperature T , exchange constant A , the anisotropy constant K and the coupling constant $J_{\text{Co,Co}}$.

n	$T(\text{K})$	$A(\text{pJ}/\text{m})$	$K(\text{MJ}/\text{m}^3)$	$J_{\text{Co,Co}}(\text{J}/\text{m}^2)$
1	1	52.78	0.547	-0.05657
2	1	52.78	0.547	-0.03000
3	1	52.78	0.547	0.01236
1	100	50.29	0.509	-0.053234
2	100	50.29	0.509	-0.02820
3	100	50.29	0.509	0.01182
1	300	45.04	0.431	-0.04749
2	300	45.04	0.431	-0.02535
3	300	45.04	0.431	0.01044
1	500	39.53	0.355	-0.04046
2	500	39.53	0.355	-0.02082
3	500	39.53	0.355	0.00919

eters [22]. By passing zero-temperature parameters such as the exchange integrals obtained from ab-initio calculations to spin dynamics simulations, temperature dependent values for the spontaneous magnetization, the exchange constant, and the anisotropy constant can be obtained [23–25]. In addition to these bulk material properties, the interface properties are essential for treating magnetization processes in multimaterial and multilayers system. A prominent example is the coupling of ferromagnetic materials through a thin Ru layer. Depending on the layer thickness the coupling may be ferromagnetic

or antiferromagnetic [1]. Such interfaces can be described within micromagnetic theory if the energy is augmented with interface energy terms. This surface term leads to a jump of the magnetization across the interface. The coupling constant between the magnetization vectors at both sides of the interface will depend on temperature. It can be derived from the domain wall energy in the bulk and the size of the jump of the magnetization at the in-

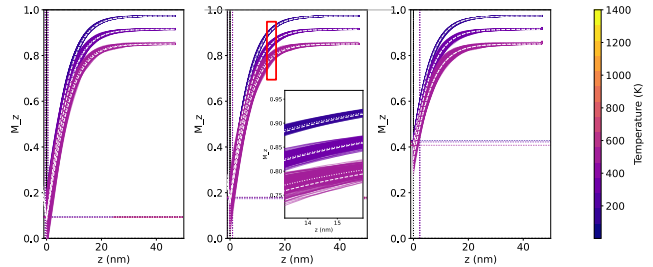


FIG. 14. Comparison of temperature dependent magnetization profiles obtained from spin dynamics and algebraic solution. The colored surfaces show the ensemble of all spin-dynamics simulations. The white dotted line is the average of those (see FIG. 9), the dashed white line demonstrate the results from algebraic solution. Left and Mid: Antiferromagnetic coupling across one and two monolayers Ru. Right: Ferromagnetic coupling across three monolayer Ru atoms. Note: We show only the right side of the profiles because of symmetry.

terface. The latter can be computed from spin dynamic simulations.

We showed how to derive both the temperature-dependent bulk properties and the temperature-dependent coupling constant for Co/Ru/Co from ab-initio and spin dynamics simulations. We assume a need of more spin dynamics simulations to improve the match between micromagnetic theory at elevated temperatures.

V. ACKNOWLEDGMENTS

We gratefully acknowledge the financial support by the Austrian Science Fund (FWF) I 5712. This work was supported by the project e-INFRA CZ (ID : 90254) for CPU time resources and the QM4ST project ($CZ.02.01.01/00/22.008/0004572$) by the Ministry of Education, Youth and Sports of the Czech Republic and by Grant No. 22 – 35410K by the Czech Science Foundation.

[1] S. Parkin, N. More, and K. Roche, Oscillations in exchange coupling and magnetoresistance in metallic superlattice structures: Co/ru, co/cr, and fe/cr, Physical review letters **64**, 2304 (1990).

[2] T. McKinnon, B. Heinrich, and E. Girt, Spacer layer thickness and temperature dependence of interlayer exchange coupling in co/ru/co trilayer structures, Physical Review B **104**, 024422 (2021).

- [3] R. Skomski, in *LNP 569*, edited by M. Thornton and M. Ziese (Springer, Berlin, Heidelberg, 2001) Chap. 10 Micromagnetic Spin Structure, pp. 204–231.
- [4] I. Turek, J. Kudrnovský, V. Drchal, P. Bruno, and S. Blügel, Ab initio theory of exchange interactions in itinerant magnets, *physica status solidi (b)* **236**, 318 (2003), <https://onlinelibrary.wiley.com/doi/pdf/10.1002/pssb.200301671>.
- [5] R. Moreno, R. F. L. Evans, S. Khmelevskiy, M. C. Muñoz, R. W. Chantrell, and O. Chubykalo-Fesenko, Temperature-dependent exchange stiffness and domain wall width in Co, *Phys. Rev. B* **94**, 104433 (2016).
- [6] G. Kresse and J. Furthmüller, Efficient iterative schemes for ab initio total-energy calculations using a plane-wave basis set, *Phys. Rev. B* **54**, 11169 (1996).
- [7] G. Kresse and D. Joubert, From ultrasoft pseudopotentials to the projector augmented-wave method, *Phys. Rev. B* **59**, 1758 (1999).
- [8] P. E. Blöchl, Projector augmented-wave method, *Phys. Rev. B* **50**, 17953 (1994).
- [9] J. P. Perdew, K. Burke, and M. Ernzerhof, Generalized gradient approximation made simple, *Phys. Rev. Lett.* **77**, 3865 (1996).
- [10] H. J. Monkhorst and J. D. Pack, Special points for Brillouin-zone integrations, *Phys. Rev. B* **13**, 5188 (1976).
- [11] M. Methfessel and A. T. Paxton, High-precision sampling for Brillouin-zone integration in metals, *Phys. Rev. B* **40**, 3616 (1989).
- [12] R. P. Feynman, Forces in molecules, *Phys. Rev.* **56**, 340 (1939).
- [13] P. Vinet, J. R. Smith, J. Ferrante, and J. H. Rose, Temperature effects on the universal equation of state of solids, *Phys. Rev. B* **35**, 1945 (1987).
- [14] W. Brown, *Micromagnetics* (Interscience Publishers, 1963).
- [15] A. Hubert and R. Schäfer, *Magnetic domains: the analysis of magnetic microstructures* (Springer Science & Business Media, 2008).
- [16] O. Fruchart, Lecture notes on nanomagnetism (2011).
- [17] Z. Lu, P. Visscher, and W. Butler, Domain wall switching: Optimizing the energy landscape, *IEEE transactions on magnetics* **43**, 2941 (2007).
- [18] H. B. Callen and E. Callen, The present status of the temperature dependence of magnetocrystalline anisotropy, and the $1/(1+\tau)^2$ power law, *Journal of Physics and Chemistry of Solids* **27**, 1271 (1966).
- [19] P. Asselin, R. F. L. Evans, J. Barker, R. W. Chantrell, R. Yanes, O. Chubykalo-Fesenko, D. Hinzke, and U. Nowak, Constrained Monte Carlo method and calculation of the temperature dependence of magnetic anisotropy, *Phys. Rev. B* **82**, 054415 (2010).
- [20] J. E. Dennis Jr, D. M. Gay, and R. E. Welsch, Algorithm 573: NLSOL—an adaptive nonlinear least-squares algorithm [e4], *ACM Transactions on Mathematical Software (TOMS)* **7**, 369 (1981).
- [21] B. M. Adams, W. J. Bohnhoff, K. R. Dalbey, M. S. Ebeida, J. P. Eddy, M. S. Eldred, R. W. Hooper, P. D. Hough, K. T. Hu, J. D. Jakeman, *et al.*, *Dakota, a multilevel parallel object-oriented framework for design optimization, parameter estimation, uncertainty quantification, and sensitivity analysis: version 6.13 user's manual*, Tech. Rep. (Sandia National Lab.(SNL-NM), Albuquerque, NM (United States), 2020).
- [22] R. Skomski, P. Kumar, G. C. Hadjipanayis, and D. J. Sellmyer, Finite-temperature micromagnetism, *IEEE transactions on magnetics* **49**, 3229 (2013).
- [23] U. Atxitia, D. Hinzke, O. Chubykalo-Fesenko, U. Nowak, H. Kachkachi, O. N. Mryasov, R. Evans, and R. W. Chantrell, Multiscale modeling of magnetic materials: Temperature dependence of the exchange stiffness, *Physical Review B—Condensed Matter and Materials Physics* **82**, 134440 (2010).
- [24] P. Nieves, S. Arapan, T. Schrefl, and S. Cuesta-Lopez, Atomistic spin dynamics simulations of the MnAl τ -phase and its antiphase boundary, *Physical Review B* **96**, 224411 (2017).
- [25] S. Westmoreland, R. Evans, G. Hrkac, T. Schrefl, G. Zimanyi, M. Winklhofer, N. Sakuma, M. Yano, A. Kato, T. Shoji, *et al.*, Multiscale model approaches to the design of advanced permanent magnets, *Scripta Materialia* **148**, 56 (2018).